Nanoscale infrared imaging analysis of carbonaceous chondrites: Understanding organic-mineral interactions during aqueous alteration

Yoko Kebukawa[1]*, Hanae Kobayashi[2], Norio Urayama[2], Naoki Baden[2], Masashi Kondo[3], Michael E. Zolensky[4], and Kensei Kobayashi[1]

*Corresponding author: kebukawa@ynu.ac.jp

[1]Faculty of Engineering, Yokohama National University, 79-5 Tokiwadai, Hodogaya-ku, Yokohama 240-8501, Japan

[2]Nihon Thermal Consulting, 1-5-11 Nishishinjuku, Sinjuku-ku, Tokyo 160-0023, Japan

[3]Instrumental Analysis Center, Yokohama National University, 79-5 Tokiwadai, Hodogaya-ku, Yokohama 240-8501, Japan

[4]ARES, NASA Johnson Space Center, 2101 NASA Parkway, Houston, TX 77058, USA

Abstract

Organic matter in carbonaceous chondrites is distributed in fine grained matrix. To understand pre- and post-accretion history of organic matter and its association with surrounding minerals, microscopic techniques are mandatory. Infrared (IR) spectroscopy is a useful technique, but the spatial resolution of IR is limited to a few micrometers, due to the diffraction limit. In this study, we applied the high spatial resolution IR imaging method to CM2 carbonaceous chondrites Murchison and Bells, that is based on an atomic force microscopy (AFM) with its tip detecting thermal expansion of a sample resulting from absorption of infrared radiation. We confirmed that this technique permits for the first time ~20 nm special resolution organic analysis for the meteorite samples. The IR imaging confirmed the previously reported association of organic matter and phyllosilicates at much higher spatial resolution. This was the first observation of heterogeneous distributions of organic matter in the functional group, revealing its association with minerals at ~20 nm spatial resolution in meteorite samples. Our results further imply that the associated mineral species play a crucial role in the molecular structures of OM.

Keywords: Meteorites, IR spectroscopy, AFM-IR, Organic matter

Significance

Spatial relationships between organic matter and minerals are necessary for understanding the formation and evolution of organic matter during aqueous and thermal alteration in their parent bodies, as well as pre-accretional history. Infrared (IR) spectroscopy is a powerful tool to analyze the molecular structures of organic matter and identification of minerals. However, its spatial resolution is limited due to the diffraction limit. Recently, the atomic force microscopy (AFM) based IR nano-spectroscopy was developed and applied in various scientific fields, to overcome the diffraction limit of IR. We applied the AFM based IR nano-spectroscopy to carbonaceous chondrites and studied organic-mineral associations at the ~20 nm spatial resolution for the first time.

Primitive extraterrestrial materials such as carbonaceous chondrites contain diverse organic matter (OM). Although distinct organic grains called “nanoglobules” 100 nm to 1 μm in size are often found in primitive carbonaceous chondrites (1, 2), they consist of roughly 10% or less of the total organics in chondrites (3). The remaining organics are smaller than “nanoglobules” and distributed in fine-grained matrix. In order to understand pre- and post-accretion history of OM and its interaction with associated minerals, microscopic techniques are mandatory. Scanning electron microscope (SEM) observation with osmium labeling has demonstrated that OM in carbonaceous chondrites is associated with clay minerals, which may have had important trapping and possibly catalytic roles in the evolution of organics in the early solar system (4).

To obtain molecular structure information at the submicron scale, scanning transmission X-ray microscopy (STXM) combined with carbon X-ray absorption near-edge structure spectroscopy (C-XANES) is so far the most suitable method. The STXM with C-XANES provides molecular structure information at the ~40 nm spatial resolution, and is often applied to various extraterrestrial materials including carbonaceous chondrites (5-12), Antarctic micrometeorites (AMMs) (13, 14), interplanetary dust particles (IDPs) (15, 16), and cometary particles recovered from Comet 81P/Wild 2 by the STARDUST mission (17-20).

Fourier transform infrared (FTIR) microspectroscopy is a well-established technique for extraterrestrial materials (15-17, 21-27), as well as imaging analyses (28-32). IR spectroscopy provide information of not only molecular structures of OM similar to C-XANES, but also mineral identification, and thus could be a complementary method to STXM/C-XANES. However, the spatial resolution of IR is limited to a few micrometer (roughly equal to wavelength), due to the diffraction limit. The scanning near-field optical microscopy (SNOM) technique allows one to obtain IR spectra at sub-micrometer spatial resolution (33). We have applied near-field IR micro-spectroscopy to carbonaceous chondrites and demonstrated organic-phyllosilicates associations (28, 29). However, the

optics and probe setting were not completely sufficient to detect pure near-field signals and thus the spatial resolution was limited to ~1 μm. Dominguez et al. (34) reported on sub-micron (~20 nm) mineral identification of the Murchison meteorite and a cometary dust particle with near-field IR imaging using suitable background (i.e., non-near field scatterings) suppression, but the wavelength (wavenumber) range was limited to 800-1100 cm^{-1}, which did not cover characteristic organic absorptions.

Alternatively, a high spatial resolution IR imaging technique which detects photothermal induced resonance using a tunable laser combined with an atomic force microscope was recently developed and applied to various research fields (35-37). When light is absorbed by the sample, the temperature increase causes a characteristic thermal expansion. This thermal expansion drives the cantilever into oscillation. The oscillation amplitude of the cantilever is directly proportional to the amount of light absorbed. The technique covers full mid-IR including ranges for organic absorption features. Here we report IR imaging analyses of carbonaceous chondrites by atomic force microscopy-based infrared spectroscopy (AFM-IR) that provides IR imaging with spatial resolution far below conventional optical diffraction limits.

Results

Murchison meteorite

IR absorption spectra (Fig. 1a,b) of the Murchison meteorite were obtained using the nanoIR at locations indicated in Fig. 1c. The IR spectra indicated in red showed absorption bands at approximately 3400 cm^{-1} and 1640 cm^{-1}, and are assigned to structural and/or absorbed H_2O of hydrous silicates, at 2960, 2930 and 2860 cm^{-1}, assigned to the aliphatic C-H stretching modes, at around 1435 cm^{-1}, assigned to CO_3^{2-} of carbonates, at around 1150 cm^{-1}, assigned to SO_4^{2-} of sulfates, and at around 1000 cm^{-1}, assigned to the Si-O stretching modes of silicates. The spot in green (Fig. 1c) was dominated by sulfates with lesser silicates, and spots in blue are mainly silicates with less OH and sulfates. These features were mostly consistent with the IR spectra of the Murchison meteorite

obtained with conventional micro-FTIR (Fig. 2). However, the NanoIR spectra reflected more local characteristics, e.g., a spot with abundant aliphatic CH and sulfates that are less significant in the conventional micro-FTIR spectra obtained for larger areas (100 × 100 μm^2). It should be noted that amplitude powers were not linear to wavenumbers, i.e., higher power was applied at the region of aliphatic CH, thus the peak intensities were enhanced.

Fig. 3 shows 3 × 3 μm^2 IR absorption maps with the IR source tuned to 1000 cm^{-1} corresponding to SiO, 1150 cm^{-1} corresponding to sulfates, 1730 cm^{-1} corresponding to C=O, 2920 cm^{-1} corresponding to aliphatic CH_2, 2960 cm^{-1} corresponding to aliphatic CH_3, and 3400 cm^{-1} corresponding to OH. Some part of the silicates (lower right in Fig. 3a) overwrapped with the OH-rich area that indicated phyllosilicates. Fig. 4 shows the CH_2/CH_3 peak intensity ratio map generated from 2920 cm^{-1} (CH_2) map and 2960 cm^{-1} (CH_3) map after image shift correction using the AFM image.

Bells meteorite

IR absorption spectra (Fig. 5a,b) of the Bells meteorite were obtained using the nanoIR at locations indicated in Fig. 5c. None of the five points showed the OH absorption band in this area. One of these points showed dominant absorptions at around 2950 cm^{-1} assigned to aliphatic C-H, as well as at ~1730 cm^{-1} assigned to C=O, ~1600 cm^{-1} assigned to aromatic C=C, at around 1450 cm^{-1} assigned to carbonates, at ~1200 cm^{-1} assigned to sulfates and/or C-O, and at ~950 cm^{-1} assigned to silicates. The other spots showed dominant silicate peaks at around 1000 cm^{-1}, and some peaks at 1450 cm^{-1}, 1200 cm^{-1} and 1150 cm^{-1}. It should be noted that the amplitude power at aliphatic C-H region was 5.4 times higher than the silicate region, and thus the peak intensities of aliphatic regions were enhanced compared to the silicate region. The nanoIR spectra did not resemble the IR spectra of the Bells meteorite obtained by the conventional technique (Fig. 2), probably due to heterogeneities of the meteorite since the analyzed area was only 2 × 1 μm^2.

Fig. 6 shows 2 × 1 μm^2 IR absorption maps with the IR source tuned to 1010 cm^{-1} corresponding to SiO, 1124 cm^{-1} corresponding to sulfates, 1450 cm^{-1} corresponding to carbonates, 1724 cm^{-1}

corresponding to C=O, 2920 cm^{-1} corresponding to aliphatic CH_2, 2960 cm^{-1} corresponding to aliphatic CH_3, and 3400 cm^{-1} corresponding to OH. Fig. 7 shows the CH_2/CH_3 peak intensity ratio map generated from 2920 cm^{-1} (CH_2) map and 2960 cm^{-1} (CH_3) map after image shift correction.

Antigorite as a contamination control

IR spectra of phyllosilicate rich samples are known to be susceptible to contamination from environmental OM (38). Thus, we prepared antigorite (Mg-rich serpentine) heated at 500 °C for 4 hours as a contamination control sample and analyzed in the same manner as the meteorite samples (antigorite samples were prepared only on an Au coated mirror). The nanoIR spectra of the heated antigorite showed a peak at 3660 cm^{-1} and 1080 cm^{-1} assigned to OH and SiO, respectively, but no organic peaks were observed (Fig. 8). Fig. 9 shows an IR map of heated antigorite for 2920 cm^{-1} (aliphatic CH_2) in 6 × 2 μm^2 region. The concentration of aliphatic CH_2 was below detection limits. Thus, we concluded that our meteorite data was not affected by organic contamination during the analysis procedures.

Discussion

Spatial resolution

The diffraction limit is generally roughly equivalent to the wavelength, e.g., ~3.3 μm at 3000 cm^{-1} and ~10 μm at 1000 cm^{-1}. Point spectra a few micrometer-sized areas from our meteorite samples (Figs. 1 and 5) clearly showed that the spatial resolution in our nanoIR analysis was beyond the diffraction limit. The IR maps (Figs. 2 and 6) also confirmed that the actual spatial resolution was at least 20 nm. This is much higher spatial resolution as compared to previous IR imaging measurements using near-field IR (28, 29) and synchrotron-based IR (30-32).

CH_2/CH_3 ratios

The CH_2/CH_3 peak intensity ratio is a good indicator of aliphatic chain length and branching.

147 Although the CH_2/CH_3 peak intensity ratio is not equal to the molar abundance ratio of CH_2/CH_3 due
148 to the difference of molar absorption coefficients between CH_2 and CH_3, the CH_2/CH_3 peak intensity
149 ratio shows a linear correlation with the actual number of CH_2/CH_3 in molecules (39).

150 The CH_2/CH_3 peak intensity ratio of the Murchison meteorite is 1.0 ± 0.1 and that of the Bells
151 meteorite is 1.4 ± 0.2 (29). The average CH_2/CH_3 peak intensity ratio (average of the points that have
152 2920 cm^{-1} intensity over 0.005) of the Murchison meteorite obtained from the CH_2/CH_3 map (Fig. 4)
153 was 1.2 ± 0.4. This is consistent with the reported ratio for Murchison (1.0 ± 0.1) (29), within analytical
154 error. The average CH_2/CH_3 peak intensity ratio of Bells (Fig. 7) was 0.7 ± 0.4 (average of the points
155 that have 2960 cm^{-1} intensity over 0.02). This is lower than the reported ratio of Bells meteorite (1.4 ±
156 0.2) (29). Considering the small analyzed area (2 × 1 μm^2), this difference could due to heterogeneity
157 of OM in the Bells meteorite. Further presumption could be made that the OM associated with
158 anhydrous matrix phases has lower CH_2/CH_3 ratio compared to bulk OM that is primarily associated
159 with hydrated phases (phyllosilicates) (28, 29). Further discussion regarding the distribution of the
160 CH_2/CH_3 peak ratios and their association with minerals are in the following sections of this paper.
161
162 ***Murchison meteorite***

163 In the IR maps of the Murchison meteorite (Fig. 3), ~1.5 μm of the sulfate region is surrounded by
164 silicates. OH-rich region is in the lower right (Fig. 3f), and thus the silicates in this region are likely
165 hydrated, i.e., phyllosilicates. The silicate-rich regions without OH are likely anhydrous silicates, most
166 likely olivine and pyroxene. Note that adsorbed water from the atmosphere would contribute to the
167 OH band, but anhydrous silicates typically do not show a significant OH band as compared to
168 phyllosilicates because structural OH in phyllosilicates enhances atmospheric water adsorption. IR
169 absorptions from organics (Fig. 3c,d,e) overlap with phyllosilicates. These results are consistent with
170 the previous IR imaging measurements of carbonaceous chondrites that showed an association of OM
171 with phyllosilicates (28, 29, 31, 32), but our results demonstrate this association at much higher spatial
172 resolution. This indicates that the OM is finely mixed with phyllosilicates, and that perhaps OM exists

in the interlayer spacings. The high CH_2/ CH_3 rich spots (<~100 nm) are observed in aliphatic rich regions (lower right in Fig. 4). This is the first time that the heterogeneity of CH_2/CH_3 ratio was observed at the scale of a few 10's of nm, suggesting a heterogeneous formation process of OM or mixing of OM of different origins.

The matrix of Murchison is composed largely of tochilinite and cronstedtite (serpentine), along with minor amounts of other phases such as olivine, enstatite, pyrrhotite, pentlandite, magnetite and calcite (40). This mineralogy is consistent with our IR map showing hydrous and anhydrous silicates. However, sulfates are not so common in CM chondrites, and it is possible that these sulfates could be terrestrial weathering products (41), as pointed out by Gounelle and Zolensky (42) for sulfate veins in CI chondrites. Thus, the sulfates in our Murchison sample may have originated from hydrolysis of sulfides such as pyrrhotite and pentlandite, and/or by oxidation during preservation or during ultramicrotomy due to use of water.

There are small spots rich in C=O. One was ~100 nm at the upper middle of the map, and the other was ~30 nm at the middle left (Fig. 3c). Both consist of multiple pixels, and thus they should not be artifacts. One of these C=O rich spots (the smaller one) also shows a high abundance of aliphatic CH_2 (Fig. 3d) and thus appears as a hot spot in the CH_2/CH_3 ratio map (Fig. 4). These spots (~30-100 nm) could be nanoglobules. Typical nanoglobules in Murchison are aromatic-rich or have insoluble organic matter (IOM) like compositions (5). Although they have some C=O, predominantly C=O rich nanoglobules have not been found so far. However, the C=O rich spots in Murchison were rich in C=O as compared to OM in other areas which mostly represent IOM. The details for these compounds are not known since we do not have full IR spectra of them, although IR spectroscopy of bulk meteorites is not ideal for aromatic features since they overlap with water etc. To see the heterogeneity of nanoglobule-like OM, further measurements are required with increasing analytical areas as well as a full spectrum for each compound. Considering that these features are not found in the control sample (heated antigorite), they are not likely to be laboratory contamination.

Bells meteorite

In the IR maps of the Bells meteorite, OH absorption is not observed in the analytical area (2 × 1 μm^2). There are several areas, around 200-300 nm each, with strong absorptions of silicates; 1D, 4F, 1H and 2F (Fig. 6a). The corresponding AFM images show that the heights of these regions (except 2F) are significantly low. Hence, it is probably due to enhancement of IR absorption by Au on the surface of the substrate (43). Note that the Murchison sample is mounted on ZnS, thus such enhancement is not observed. Silicates and sulfates interdigitately distribute at 200-300 nm scale in the left region (Fig. 6a,b). Sulfates are more finely mixing or overlapping with silicates in the right region. Carbonates are largely overlapped with sulfates, except some areas in 1G and 3E (Fig. 6b,c).

The Bells meteorite is a highly brecciated, unusual CM2 chondrite. The fine-grained mineralogy of matrix in Bells differs considerably from other CM chondrites and has closer affinities to matrix in CI chondrites (44). The dominant phases are fine-grained saponite interlayered with serpentine. Tochilinite and cronstedtite, which are typical of CM chondrite matrix, are entirely absent (44). Fragmental olivines and pyroxenes are common, pentlandite, pyrrhotite, magnetite, anhydrite, calcite, and rare Ti-oxides also occur as accessory phases (44). The magnetite is more abundant than in other CMs. Considering this mineralogy, the nanoIR analytical area (2 × 1 μm^2) apparently does not represent the average matrix mineralogy of Bells. We do not see any hydrous phases in the analytical area. The silicates in the IR map are likely olivines and/or pyroxenes. Sulfates in the IR map could be anhydrite or oxidation products from sulfides, e.g., pentlandite and pyrrhotite.

IR absorptions of OM are observed in the green lined area (Fig. 6d,e,f). The OM in Bells appears as a vein-like structure present at grain boundaries. Unlike phyllosilicates in Murchison, anhydrous silicates in Bells do not show significant association with OM. Rather, OM is associated with carbonates and sulfates. The C=O and aliphatic CHs are heterogeneously distributed in the OM-rich area. The upper region (2E to 1G) is relatively C=O rich and the lower region (4E) is relatively aliphatic-rich. The area around 1D shows strong absorptions of both C=O and aliphatics, due probably to enhancement by Au. The C=O rich region is also rich in sulfates and carbonates but contains few

225 silicates. The aliphatic-rich region (4E) is rich in sulfates, carbonates and some silicates.

226 C=O rich OM areas (1G and 2E) do not overlap with silicates, but an aliphatic-rich OM area (4E)
227 has some silicates. This could be due to the hydrophobic nature of aliphatic moieties compared to C=O,
228 and thus aliphatic-rich OM is preferentially associated with anhydrous phases. There is also a
229 possibility that some of aliphatic-rich OM could have originated from anhydrous processes, such as
230 interstellar ice chemistry (45, 46). This explanation is consistent with the observation that anhydrous,
231 chondritic IDPs tend to rich in aliphatic moieties (15, 16). C=O rich OM could have originated from
232 aqueous activities. Cody et al. (47) reported that IOM-like organic solids could have been produced
233 from formaldehyde. Such organic solids tend to be rich in C=O, particularly synthesized in lower
234 temperatures, in their IR spectra (48).

235 The OM in the observed area in the Bells meteorite has a lower CH_2/CH_3 peak intensity ratio ($0.7 \pm$
236 0.4) compared to the OM in Murchison associated with phyllosilicates (1.2 ± 0.4), as well as reported
237 values of bulk Bells (1.4 ± 0.2) and Murchison (1.0 ± 0.1) (29). The OM shows a large heterogeneity
238 in the CH_2/CH_3 ratio. Some spots (~100-200 nm) in D1, D2, and E4 have higher CH_2/CH_3 ratios, and
239 some spots (~200-300 nm) in G1 and E3 have lower CH_2/CH_3 ratios. The OM associated with sulfates
240 (likely terrestrial weathering products of sulfides) (4E in Figs. 5b and 6) has higher CH_2/CH_3 ratio
241 compared to the other areas.

242 The CH_2/CH_3 ratio in meteoritic OM generally increases with increasing alteration and/or
243 metamorphism (49). Thus, the OM associated with anhydrous silicates could be more primitive
244 compared to the OM associated with phyllosilicates. It is also known that phyllosilicates catalyze
245 various organic reactions (50). Further analyses as well as experimental investigations are required to
246 understand the roles of various minerals in the formation and evolution of organics in the early Solar
247 System.

248

249 **Conclusions**

250 We conducted high-resolution imaging IR analyses of two CM chondrites (Murchison and Bells

meteorites) using AFM-IR (nanoIR). We successfully achieved ~20 nm spatial resolution, that is beyond the diffraction limit. This is the first documentation of organic-mineral associations including fine scale overlapping of the OM and phyllosilicates at a scale less than 100 nm spatial resolution in extraterrestrial samples.

OM in the Murchison meteorite is clearly associated with phyllosilicates as reported previously, but our result reveals this critical association at much higher spatial resolution. The heterogeneity of CH_2/CH_3 ratio was observed at the scale of a few 10's of nm. We found were two isolated OM spots (~30 to 100 nm) very rich in C=O.

OM in the Bells meteorite showed a vein-like structure within mineral grain boundaries with some heterogeneities in C=O and aliphatics, as well as CH_2/CH_3 ratios. Phyllosilicates were apparently not likely present in the analytical area. Unlike phyllosilicates in Murchison, anhydrous silicates in Bells do not show a significant association with OM. Rather, OM is associated with carbonates and sulfates, which could be weathering products (including terrestrial) from sulfides.

The CH_2/CH_3 peak intensity ratios of OM associated with phyllosilicates in Murchison were consistent with the same ratio of bulk Murchison. However, the ratios in Bells that are not associated with phyllosilicates were lower than these of the bulk Bells and Murchison. This result indicates that the OM associated with anhydrous phases has a lower CH_2/CH_3 ratio compared to the OM associated with phyllosilicates. From the above observation we infer that associated mineral species seem to have crucial roles for the molecular structures of OM in carbonaceous chondrites.

Methods

Sample Preparation

The Murchison meteorite (CM2) and the Bells meteorite (anomalous CM2) were selected for this study, because Murchison is a typical CM2 and is the most studied meteorite for organic matter, and Bells is known to have abundant organic nanoglobules (51) and significantly D- and ^{15}N-rich IOM (52). Antigorite (Mg-rich serpentine – an abundant phase in CM chondrites) powder which was heated

277 in atmosphere at 500°C for 3 hours was used for contamination control. We prepared ultramicrotomed
278 thin sections using a sulfur-embedding method based on Nakamura-Messenger et al. (2). Grains from
279 each sample were embedded in a molten (115°C) sulfur droplet with a glass needle. The sulfur droplet
280 subsequently solidifies and is then attached onto an epoxy stub using glue. The Murchison sample was
281 sliced into ~70-90 nm-thick sections with a Leica ultramicrotome using a DIATOME diamond knife.
282 The sections were floated onto deionized water and transferred to a ZnS substrate. The Bells sample
283 and heated antigorite were sliced into ~100 nm-thick sections, and transferred to Au coated glass
284 substrates. Before analysis, the sections were mildly heated (<100°C, <15 min) until the sulfur
285 sublimated off, leaving the ultramicrotomed samples essentially intact. Such a low degree of heating
286 should not significantly affect the organics in the samples (53).
287
288 ***NanoIR***
289 The IR absorption spectra were obtained using a nanoIR2 (Anasys Instruments) which consists of a
290 tunable infrared laser (optical parametric oscillator, OPO) that is focused onto a sample in the
291 proximity of a probe tip from an AFM. The AFM cantilever oscillation amplitude is linearly dependent
292 on the IR absorption (54, 55).
293 The single spectrum data were obtained at selected points with a spectral resolution of 4 cm^{-1}. To
294 optimize the peaks from OM, the incident laser powers were set to 1.31% in the range from 900-1090
295 cm^{-1}, and 2.19% in the range from 1090-2000 cm^{-1} and 2600-3850 cm^{-1} for the Murchison meteorite.
296 For the Bells meteorite and antigorite, the incident laser powers were set to 1.44% in the range from
297 900-1060 cm^{-1}, 5.64% in the range from 1060-1210 cm^{-1}, 6% in the range from 1210-1630 cm^{-1},
298 2.77% in the range from 1630-1850 cm^{-1}, 5.64% in the range from 1850-2000 cm^{-1}, and 7.76% in the
299 range from 2600-3850 cm^{-1}.
300 For the IR maps, the laser power was set to 2.77% for all images of the Murchison meteorite. For
301 the Bells meteorite, the laser power was 1.44% for the map at 1010 cm^{-1}, 4.35% at 1124 cm^{-1}, 5.64%
302 at 1450 cm^{-1}, 2.19% at 1724 cm^{-1}, 11.06% at 2920 cm^{-1} and 2960 cm^{-1}, and 14.96% at 3400 cm^{-1}.

For antigorite, the laser power was 7.76% for the map at 2920 cm^{-1}. The scan rate was 0.1 Hz for all IR maps. AFM images were recorded during the mapping measurements to keep track of the sample drift. All AFM scans in the AFM-IR were done in contact-mode using an EX-TnIR gold coated cantilever with 0.3 V of the probe voltage.

Acknowledgements

This work was supported by Japan Society for the Promotion of Science KAKENHI (grant number JP17H02991, JP17H06458, and JP18K03722), and the Astrobiology Center of National Institutes of Natural Sciences (grant number AB281004, AB291005, and AB301020).

References

1. Garvie LAJ & Buseck PR (2004) Nanosized carbon-rich grains in carbonaceous chondrite meteorites. *Earth. Planet. Sci. Lett.* 224(3-4):431-439.
2. Nakamura-Messenger K, Messenger S, Keller LP, Clemett SJ, & Zolensky ME (2006) Organic globules in the Tagish Lake meteorite: Remnants of the protosolar disk. *Science* 314(5804):1439-1442.
3. Pizzarello S, Cooper GW, & Flynn GJ (2006) The nature and distribution of the organic material in carbonaceous chondrites and interplanetary dust particles. *Meteorites and the Early Solar System II*, eds Lauretta DS & McSween JHY (University of Arizona Press, Tucson), pp 625-651.
4. Pearson VK*, et al.* (2002) Clay mineral-organic matter relationships in the early solar system. *Meteoritics & Planetary Science* 37(12):1829-1833.
5. De Gregorio BT*, et al.* (2013) Isotopic and chemical variation of organic nanoglobules in primitive meteorites. *Meteoritics & Planetary Science* 48(5):904-928.
6. Groopman E, Nittler LR, Bernatowicz T, & Zinner E (2014) NanoSIMS, TEM, and XANES studies of a unique presolar supernova graphite grain. *The Astrophysical Journal* 790(1):9.
7. Kebukawa Y*, et al.* (2014) Diamond xenolith and matrix organic matter in the Sutter's Mill meteorite measured by C-XANES. *Meteoritics & Planetary Science* 49(11):2095-2103.
8. Le Guillou C, Bernard S, Brearley AJ, & Remusat L (2014) Evolution of organic matter in Orgueil, Murchison and Renazzo during parent body aqueous alteration: In situ investigations. *Geochim. Cosmochim. Acta* 131:368-392.
9. Kebukawa Y*, et al.* (2017) Characterization of carbonaceous matter in xenolithic clasts from the Sharps (H3.4) meteorite: Constraints on the origin and thermal processing. *Geochim.*

Cosmochim. Acta 196:74-101.
10. Vinogradoff V, *et al.* (2017) Paris vs. Murchison: Impact of hydrothermal alteration on organic matter in CM chondrites. *Geochim. Cosmochim. Acta* 212:234-252.
11. Chan QHS, *et al.* (2018) Organic matter in extraterrestrial water-bearing salt crystals. *Science Advances* 4(1):eaao3521.
12. Groopman EE & Nittler LR (2018) Correlated XANES, TEM, and NanoSIMS of presolar graphite grains. *Geochim. Cosmochim. Acta* 221:219-236.
13. Noguchi T, *et al.* (2017) Variation of mineralogy and organic material during the early stages of aqueous activity recorded in Antarctic micrometeorites. *Geochim. Cosmochim. Acta* 208:119-144.
14. Yabuta H, *et al.* (2017) Formation of an ultracarbonaceous Antarctic micrometeorite through minimal aqueous alteration in a small porous icy body. *Geochim. Cosmochim. Acta* 214(Supplement C):172-190.
15. Flynn GJ, Keller LP, Feser M, Wirick S, & Jacobsen C (2003) The origin of organic matter in the solar system: Evidence from the interplanetary dust particles. *Geochim. Cosmochim. Acta* 67(24):4791-4806.
16. Keller LP, *et al.* (2004) The nature of molecular cloud material in interplanetary dust. *Geochim. Cosmochim. Acta* 68(11):2577-2589.
17. Sandford SA, *et al.* (2006) Organics captured from comet 81P/Wild 2 by the Stardust spacecraft. *Science* 314(5806):1720-1724.
18. Cody GD, *et al.* (2008) Quantitative organic and light-element analysis of comet 81P/Wild 2 particles using C-, N-, and O-μ-XANES. *Meteoritics & Planetary Science* 43(1-2):353-365.
19. De Gregorio BT, *et al.* (2010) Isotopic anomalies in organic nanoglobules from Comet 81P/Wild 2: Comparison to Murchison nanoglobules and isotopic anomalies induced in terrestrial organics by electron irradiation. *Geochim. Cosmochim. Acta* 74(15):4454-4470.
20. De Gregorio BT, *et al.* (2011) Correlated microanalysis of cometary organic grains returned by Stardust. *Meteoritics & Planetary Science* 46(9):1376-1396.
21. Matrajt G, *et al.* (2004) FTIR and Raman analyses of the Tagish Lake meteorite: Relationship with the aliphatic hydrocarbons observed in the Diffuse Interstellar Medium. *Astronomy & Astrophysics* 416(3):983-990.
22. Kebukawa Y, Nakashima S, & Zolensky ME (2010) Kinetics of organic matter degradation in the Murchison meteorite for the evaluation of parent-body temperature history. *Meteoritics & Planetary Science* 45(1):99-113.
23. Bonal L, *et al.* (2013) Hydrogen isotopic composition of the water in CR chondrites. *Geochim. Cosmochim. Acta* 106:111-133.
24. Briani G, *et al.* (2013) Short duration thermal metamorphism in CR chondrites. *Geochim. Cosmochim. Acta* 122:267-279.
25. Matrajt G, Flynn G, Brownlee D, Joswiak D, & Bajt S (2013) The origin of the 3.4 μm feature

in Wild 2 cometary particles and in ultracarbonaceous interplanetary dust particles. *The Astrophysical Journal* 765(2):145.

26. Merouane S, Djouadi Z, & Le Sergeant d'Hendecourt L (2014) Relations between Aliphatics and Silicate Components in 12 Stratospheric Particles Deduced from Vibrational Spectroscopy. *The Astrophysical Journal* 780(2):174.
27. Quirico E*, et al.* (2014) Origin of insoluble organic matter in type 1 and 2 chondrites: New clues, new questions. *Geochim. Cosmochim. Acta* 136:80-99.
28. Kebukawa Y, Nakashima S, Nakamura-Messenger K, & Zolensky ME (2009) Submicron distribution of organic matter of carbonaceous chondrite using near-field infrared microspectroscopy. *Chem. Lett.* 38(1):22-23.
29. Kebukawa Y*, et al.* (2010) Spatial distribution of organic matter in the Bells CM2 chondrite using near-field infrared microspectroscopy. *Meteoritics & Planetary Science* 45(3):394-405.
30. Yesiltas M*, et al.* (2014) Infrared imaging spectroscopy with micron resolution of Sutter's Mill meteorite grains. *Meteoritics & Planetary Science* 49(11):2027-2037.
31. Yesiltas M & Kebukawa Y (2016) Associations of organic matter with minerals in Tagish Lake meteorite via high spatial resolution synchrotron-based FTIR microspectroscopy. *Meteoritics & Planetary Science* 51(3):584-595.
32. Yesiltas M, Peale RE, Unger M, Sedlmair J, & Hirschmugl CJ (2015) Organic and inorganic correlations for Northwest Africa 852 by synchrotron-based Fourier transform infrared microspectroscopy. *Meteoritics & Planetary Science* 50(10):1684-1696.
33. Knoll B & Keilmann F (1999) Near-field probing of vibrational absorption for chemical microscopy. *Nature* 399:134-137.
34. Dominguez G*, et al.* (2014) Nanoscale infrared spectroscopy as a non-destructive probe of extraterrestrial samples. *Nature Communications* 5.
35. Dazzi A & Prater CB (2017) AFM-IR: Technology and Applications in Nanoscale Infrared Spectroscopy and Chemical Imaging. *Chem. Rev.* 117(7):5146-5173.
36. Hassenkam T, Andersson M, Dalby K, Mackenzie D, & Rosing M (2017) Elements of Eoarchean life trapped in mineral inclusions. *Nature* 548(7665):78.
37. Strelcov E*, et al.* (2017) CH3NH3PbI3 perovskites: Ferroelasticity revealed. *Science advances* 3(4):e1602165.
38. Kebukawa Y, Nakashima S, Otsuka T, Nakamura-Messenger K, & Zolensky ME (2009) Rapid contamination during storage of carbonaceous chondrites prepared for micro FTIR measurements. *Meteoritics & Planetary Science* 44(4):545-557.
39. Igisu M*, et al.* (2009) Micro-FTIR spectroscopic signatures of Bacterial lipids in Proterozoic microfossils. *Precambrian Research* 173(1-4):19-26.
40. Bland PA, Cressey G, & Menzies ON (2004) Modal mineralogy of carbonaceous chondrites by X-ray diffraction and Mossbauer spectroscopy. *Meteoritics & Planetary Science* 39(1):3-16.

41. Brearley AJ (2006) The action of water. *Meteorites and the Early Solar System II*, eds Lauretta DS & McSween JHY (University of Arizona Press, Tucson), pp 587-624.
42. Gounelle M & Zolensky ME (2001) A terrestrial origin for sulfate veins in CI1 chondrites. *Meteoritics & Planetary Science* 36(10):1321-1329.
43. Lu F, Jin M, & Belkin MA (2014) Tip-enhanced infrared nanospectroscopy via molecular expansion force detection. *Nature Photonics* 8:307-312.
44. Brearley AJ (1995) Aqueous alteration and brecciation in Bells, an unusual, saponite-bearing, CM chondrite. *Geochim. Cosmochim. Acta* 59(11):2291-2317.
45. Herbst E & van Dishoeck EF (2009) Complex organic interstellar molecules. *Annual Review of Astronomy and Astrophysics* 47:427-480.
46. Muñoz Caro GM & Dartois E (2013) Prebiotic chemistry in icy grain mantles in space. An experimental and observational approach. *Chem. Soc. Rev.* 42(5):2173-2185.
47. Cody GD*, et al.* (2011) Establishing a molecular relationship between chondritic and cometary organic solids. *Proceedings of the National Academy of Sciences of the United States of America* 108(48):19171-19176.
48. Kebukawa Y, Kilcoyne ALD, & Cody GD (2013) Exploring the potential formation of organic solids in chondrites and comets through polymerization of interstellar formaldehyde. *The Astrophysical Journal* 771(1):19.
49. Kebukawa Y, Alexander CMOD, & Cody GD (2011) Compositional diversity in insoluble organic matter in type 1, 2 and 3 chondrites as detected by infrared spectroscopy. *Geochim. Cosmochim. Acta* 75(12):3530–3541.
50. Varma RS (2002) Clay and clay-supported reagents in organic synthesis. *Tetrahedron* 58(7):1235-1255.
51. Messenger S, Nakamura-Messenger K, & Keller LP (2008) 15N-rich organic globules in a cluster IDP and the Bells CM2 chondrite. *Lunar and Planetary Science XXXIX*:2391.
52. Alexander CMOD, Fogel M, Yabuta H, & Cody GD (2007) The origin and evolution of chondrites recorded in the elemental and isotopic compositions of their macromolecular organic matter. *Geochim. Cosmochim. Acta* 71(17):4380-4403.
53. Bassim ND*, et al.* (2012) Minimizing damage during FIB sample preparation of soft materials. *Journal of Microscopy* 245(3):288-301.
54. Dazzi A, Glotin D, & Carminati R (2010) Theory of infrared nanospectroscopy by photothermal induced resonance. *J. Appl. Phys.* 107(12):124519.
55. Lahiri B, Holland G, & Centrone A (2013) Chemical imaging beyond the diffraction limit: experimental validation of the PTIR technique. *Small* 9(3):439-445.

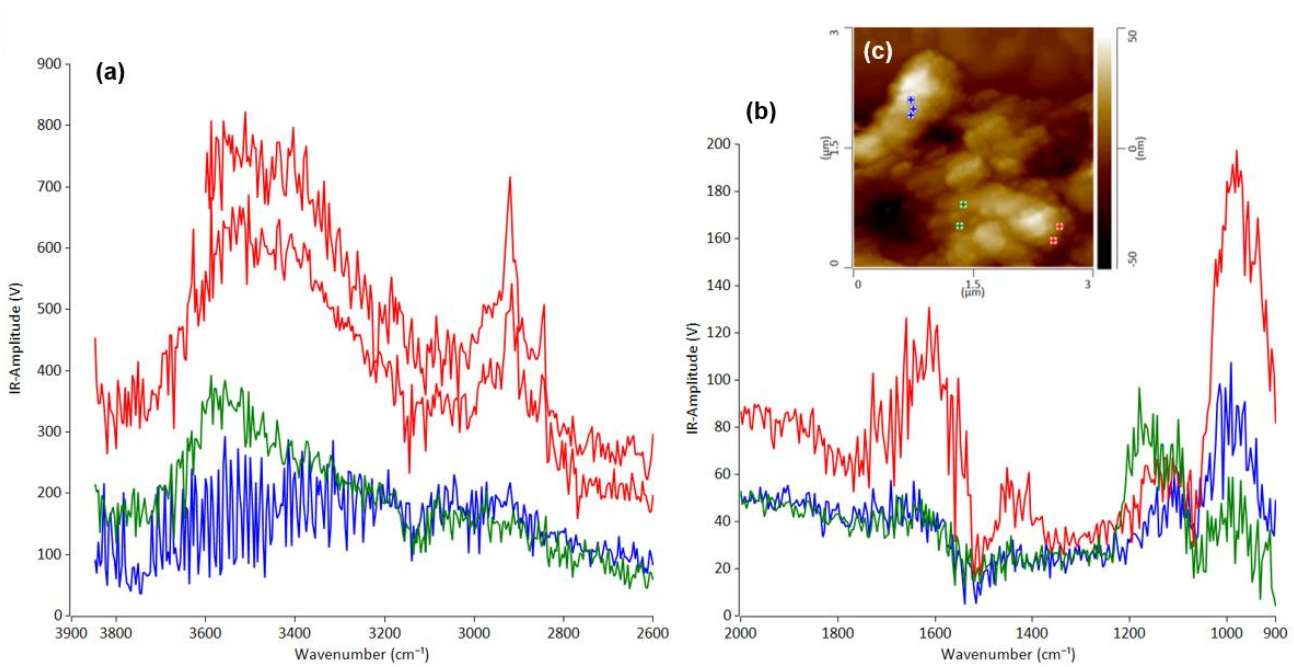

Fig. 1. IR spectra of Murchison meteorite for the region of (a) 2600-3850 cm^{-1} and (b) 900-2000 cm^{-1}. The color of the spectra correspond to the spots indicated in (c).

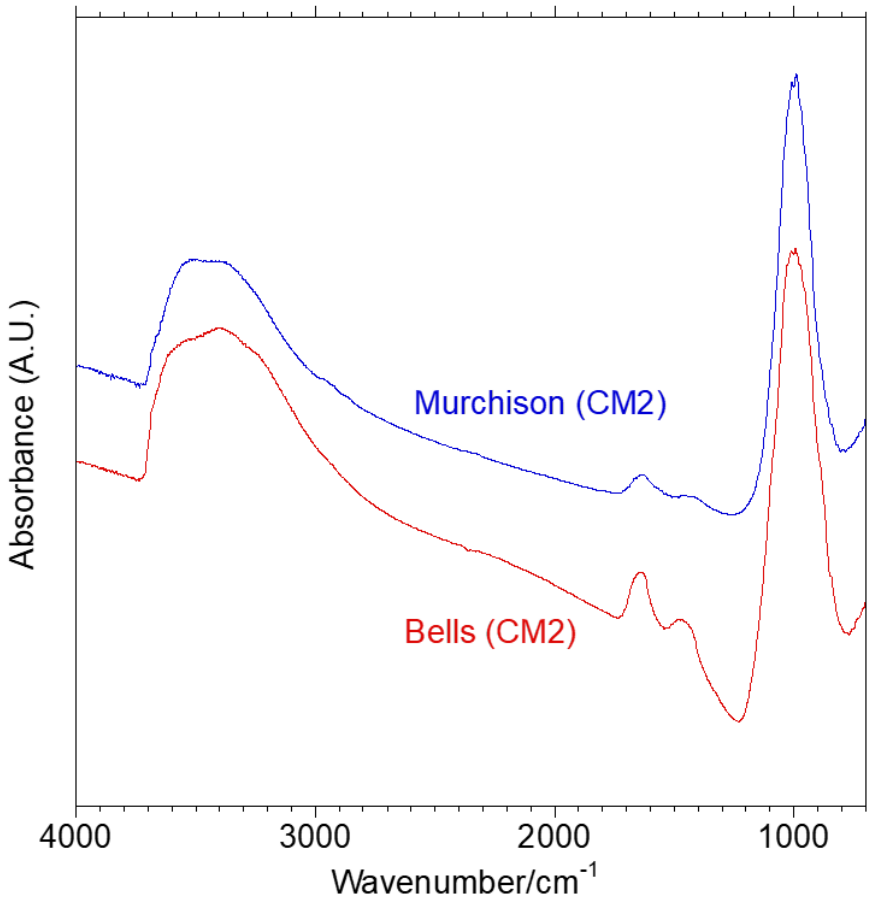

Fig. 2. IR spectra of Murchison and Bells meteorites obtained using a conventional micro-FTIR.

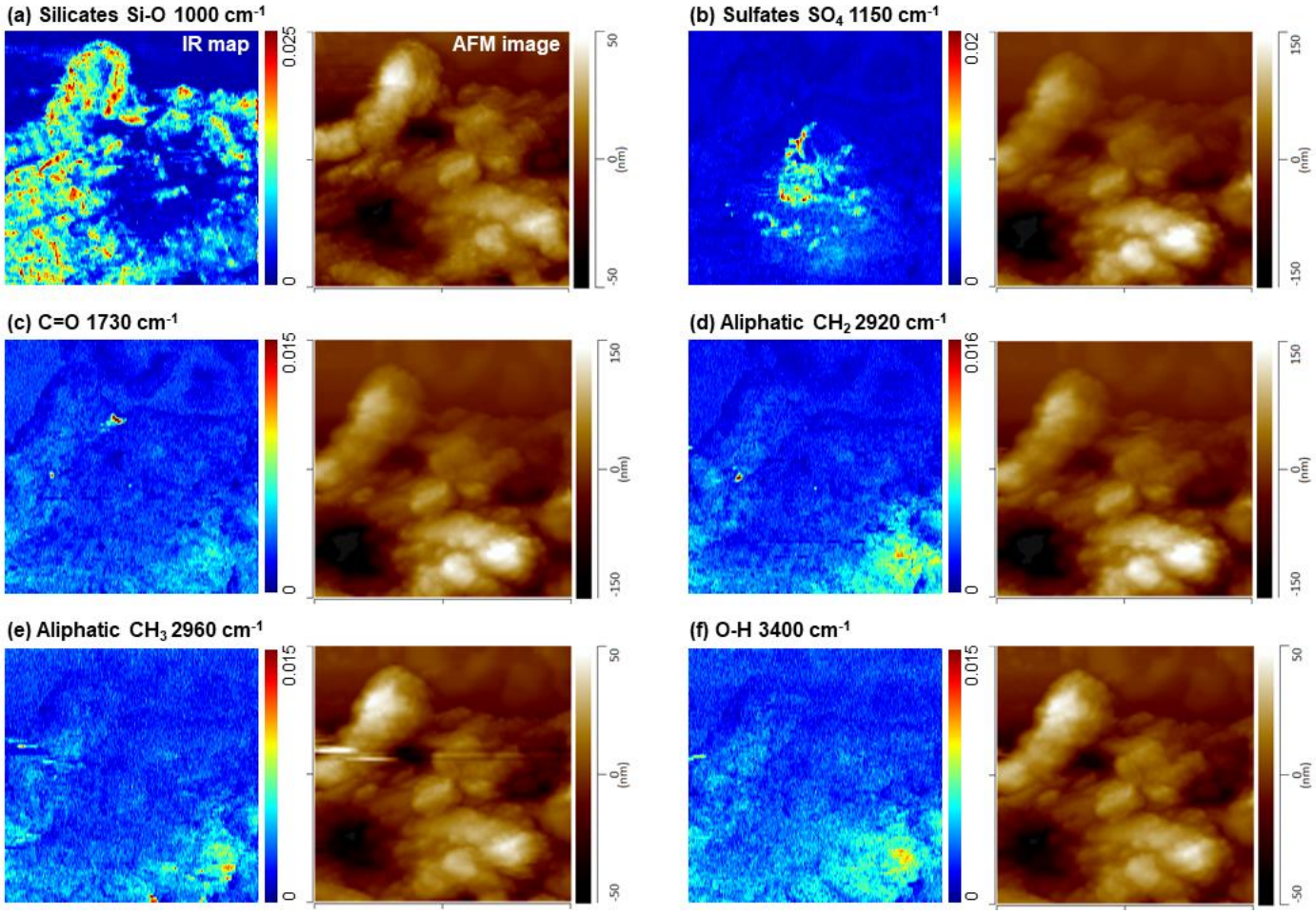

Fig. 3. IR map of Murchison meteorite for each frequency coupled with corresponding AFM image which was recorded during the mapping measurement to keep track of the sample drift. Areas are 3 × 3 μm^2 with 200 × 100 points (15 × 30 nm steps).

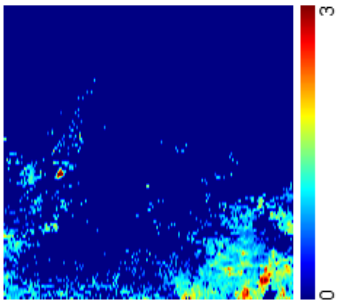

Fig. 4. The peak intensity ratio map (3 × 3 μm^2) of the Murchison meteorite for 2920 cm^{-1}/2960 cm^{-1} generated from Fig 3(d) and (e) after image shift correction. The areas with intensity over 0.005 in 2920 cm^{-1} map were calculated.

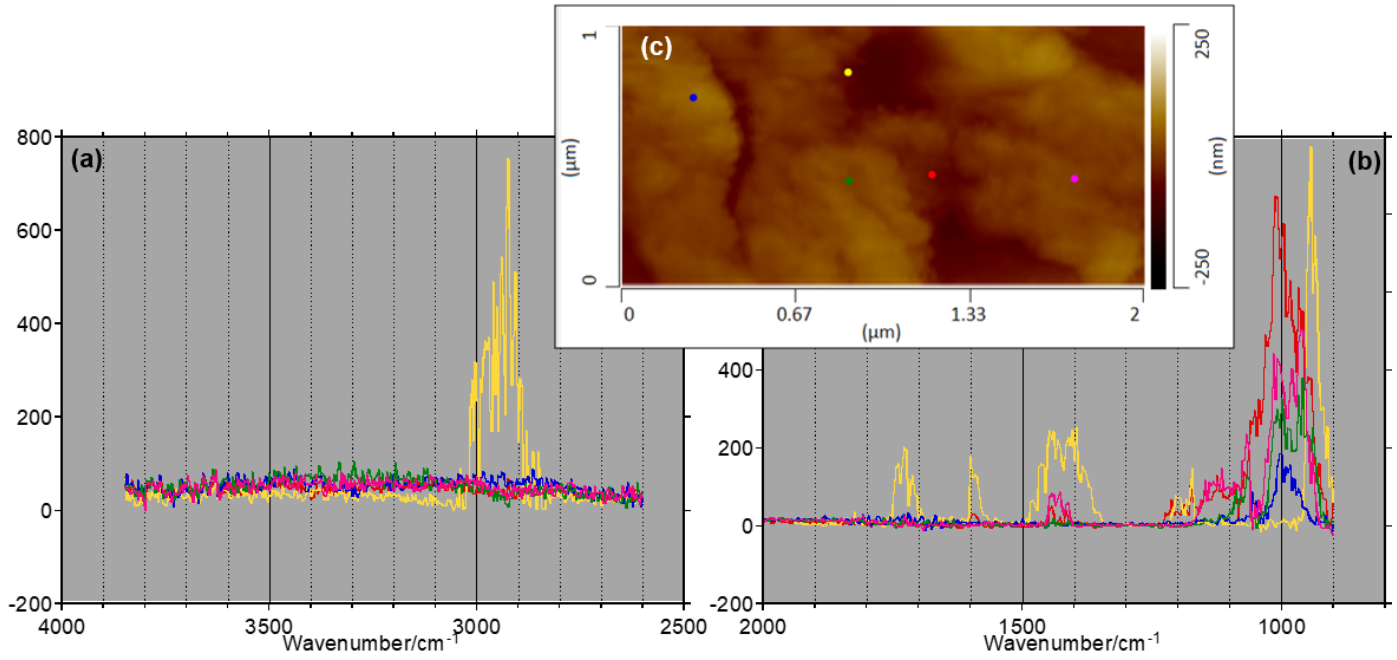

Fig. 5. IR spectra of Bells meteorite for the region of (a) 2600-3850 cm^{-1} and (b) 900-2000 cm^{-1}. The color of the spectra correspond to the spots indicated in (c).

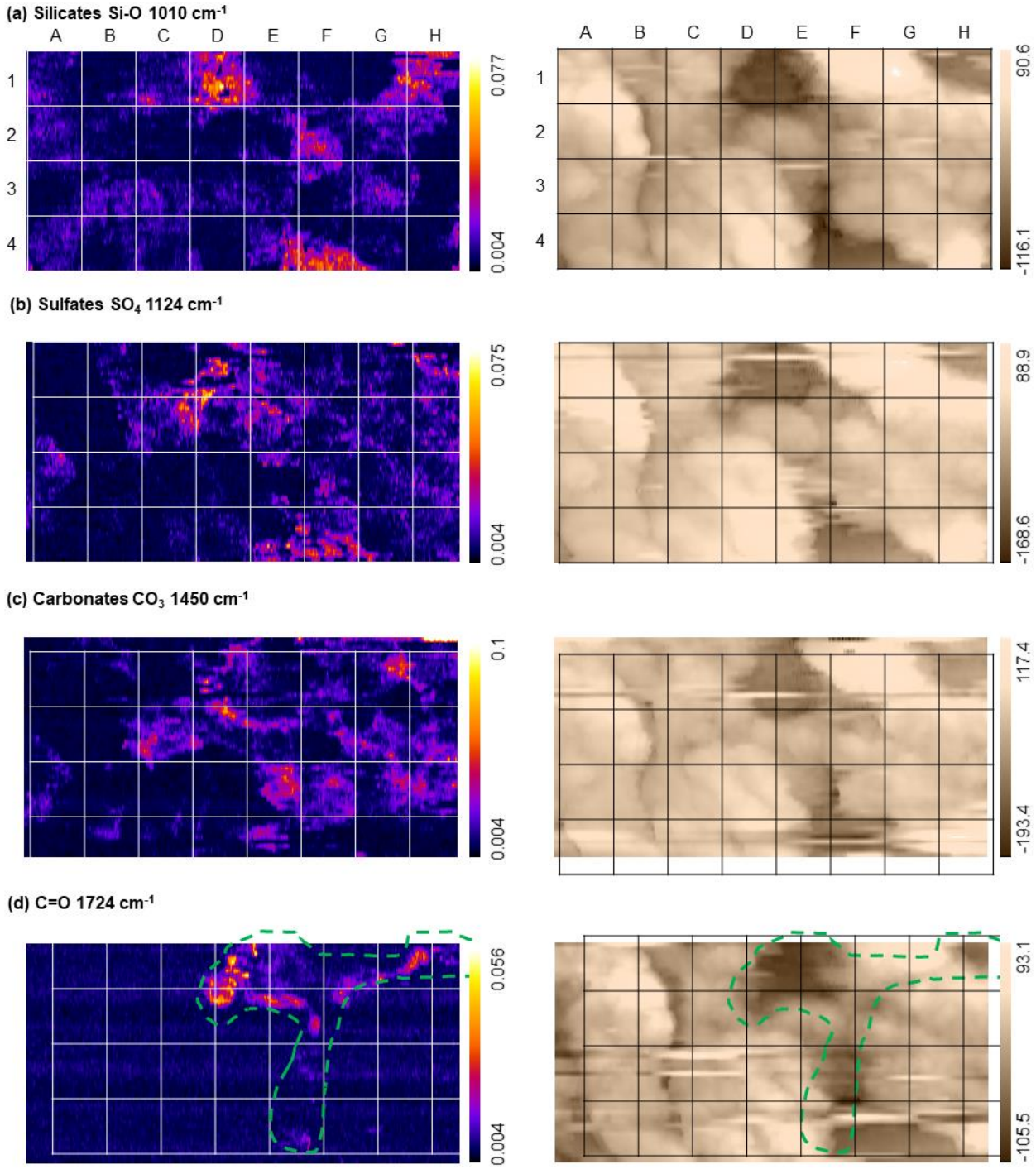
(a) Silicates Si-O 1010 cm-1
A B C D E F G H
1 2 3 4
0.077
0.004
90.6
-116.1
(b) Sulfates SO4 1124 cm-1
0.075
0.004
88.9
-168.6
(c) Carbonates CO3 1450 cm-1
0.1
0.004
117.4
-193.4
(d) C=O 1724 cm-1
0.056
0.004
93.1
-105.5

468

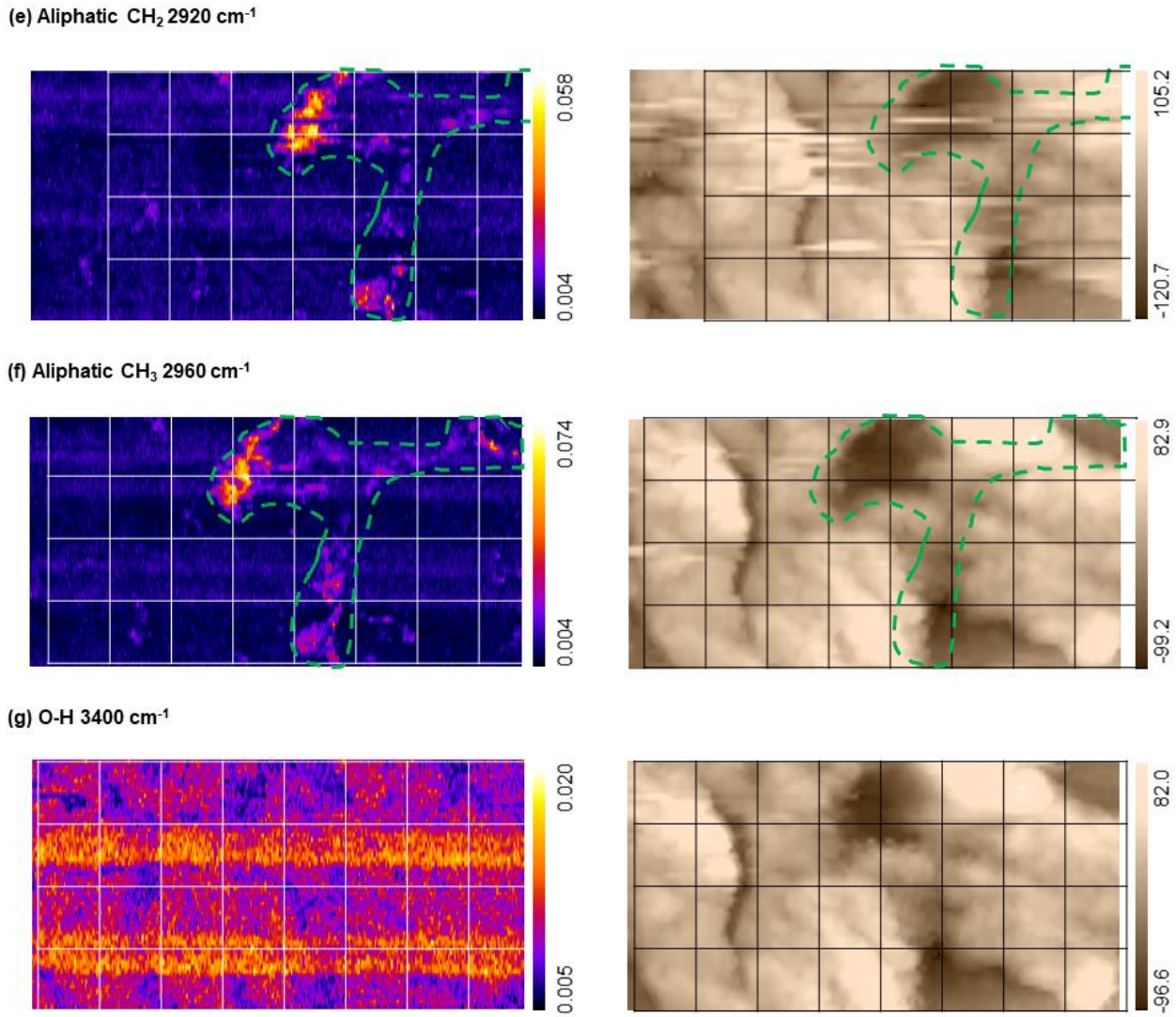

Fig. 6. IR map (left) of Bells meteorite for each frequency coupled with corresponding AFM image (right) which was obtained at the same time with an IR map to confirm sample location. Areas are 2 × 1 μm^2 with 400 × 50 points (5 × 20 nm steps). Grids are eye guides to correct the sample shifts between each scan.

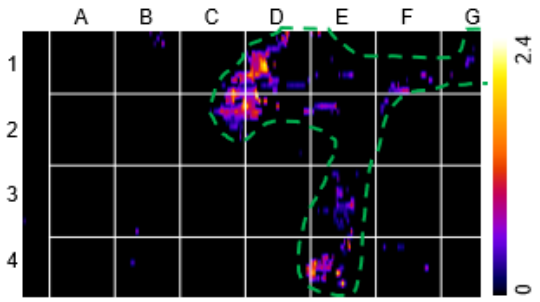

Fig. 7. The peak intensity ratio map (2 × 1 μm^2) of the Bells meteorite for 2920 cm^{-1}/2960 cm^{-1} generated from Fig 3(d) and (e) after image shift correction. The areas with intensity over 0.02 in 2960 cm^{-1} map were calculated.

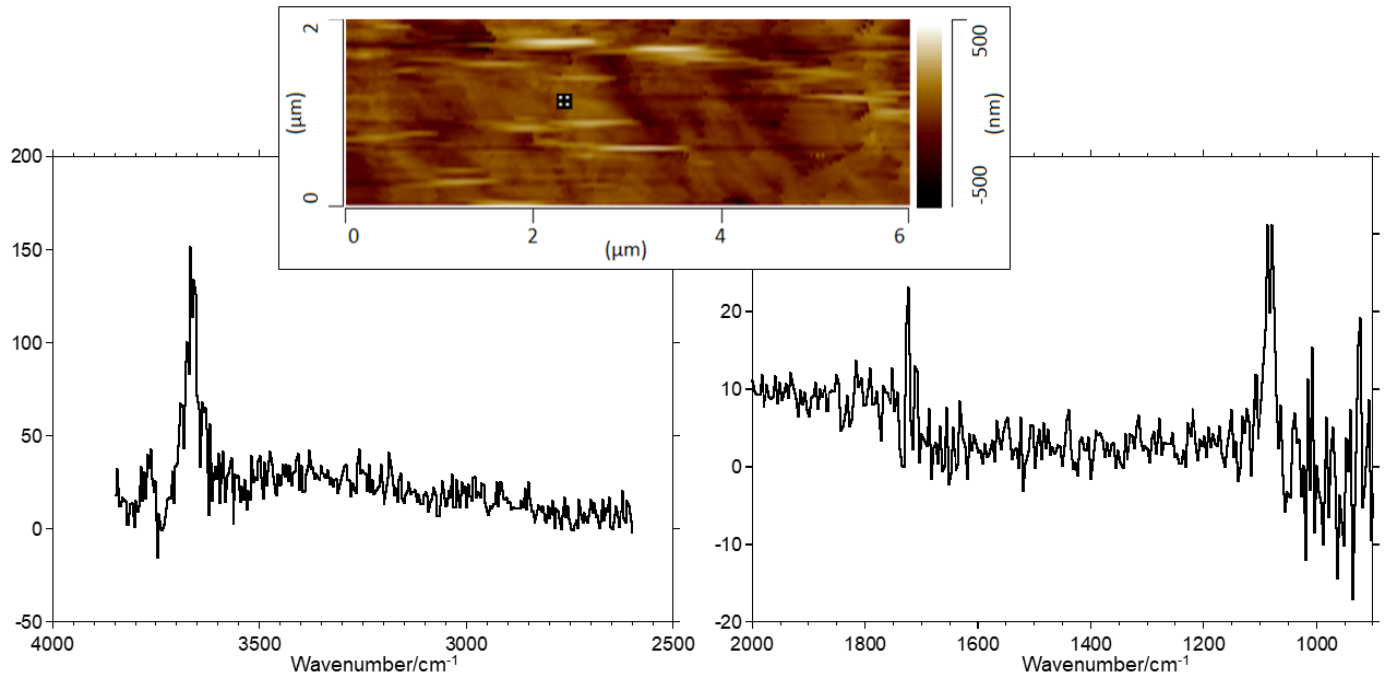

Fig. 8. IR spectra of baked antigorite for contamination control.

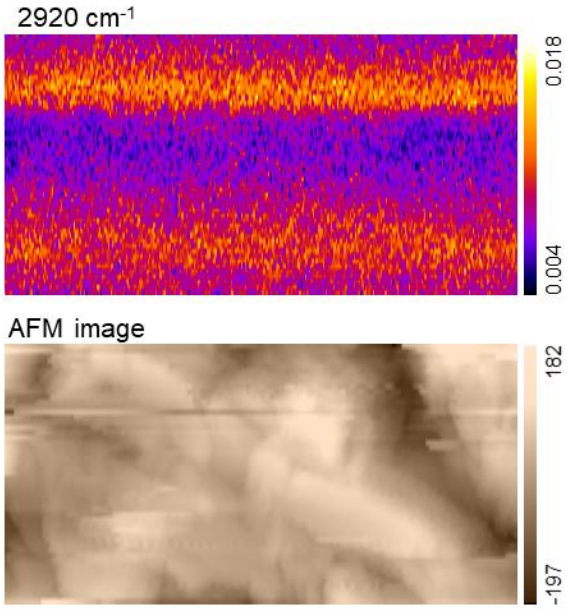

Fig. 9. IR map (top) at 2920 cm-1 of baked antigorite for contamination control with corresponding AFM image (botom) which was obtained at the same time with an IR map to confirm sample location. Areas are 2 × 1 µm^2 with 400 × 50 points (5 × 20 nm steps).